Vacuum 214 (2023) 112198

Contents lists available at ScienceDirect

Vacuum

journal homepage: www.elsevier.com/locate/vacuum

Development of non evaporable getter pumps for large hydrogen throughput and capacity in high vacuum regimes

E. Sartori [a,b,*], M. Siragusa [a], P. Sonato [a,c], F. Siviero [d], M. Mura [d], E. Maccallini [d], A. Ferrara [d], P. Manini [d], S. Hanke [e], C. Day [e]

[a] Consorzio RFX, Corso Stati Uniti 4, 35127, Padova, PD, Italy
[b] Università Degli Studi di Padova, Dept. of Management and Engineering, Stradella S. Nicola 3, 36100, Vicenza, VI, Italy
[c] Università Degli Studi di Padova, Dipartimento di Ingegneria Industriale, Via 8 Febbraio 2, I-35122, Padova, PD, Italy
[d] SAES Getters S.p.A., Viale Italia 77, 20045, Lainate, MI, Italy
[e] Karlsruhe Institute of Technology (KIT), 76344, Eggenstein-Leopoldshafen, Germany

ARTICLE INFO

Handling Editor: Oleg Malyshev

Keywords:
Non evaporable getters
High-vacuum pumps
Hydrogen absorption
Vacuum systems of particle accelerators

ABSTRACT

In vacuum technology, capture pumps based on Non Evaporable Getters are commonly applied to ultra-high vacuum systems. Recent improvements in the absorption of hydrogenic species, with the introduction of Zr–V–Ti–Al alloys (ZAO®), make them an appealing and viable solution for the application in fusion research, and in particular for the vacuum system of neutral beam injectors (hydrogen pumping speed of thousands of m^3/s, pressure of tens of mPa). This paper describes the characterization of the new NEG material in pumps of increasing dimensions, including the development, construction and test of a large mockup pump of modular design, to demonstrate the scalability of the technology. Effective pumping speeds of the order of 14 m^3/s or higher at a concentration of 130 Pa m^3/kg were achieved by the mockup pump, for an installed getter mass of about 16 kg, and a stability within 10% up to 1300 Pa m^3/kg The measured effective pumping speed per unit area of sintered disks is of the order of 3.5 m/s, corresponding to 4.9 m/s at the disk surfaces as derived from numerical simulations. General guidelines for the design of large NEG pumps for hydrogen are discussed, including thermal aspects and duty cycle of the pump.

1. Introduction

Non Evaporable Getters (NEGs) are metallic compounds able to sorb most of the active gas molecules, used as capture vacuum pumps, in the form of disks [1,2], pills or strips [3], thin films (e.g. [4] and references therein). NEG alloys were deeply studied for the possibility of modulating the getter characteristics, with typical metals including, for example, titanium, zirconium, vanadium, rare earths, etc. They are commonly used in ultrahigh vacuum conditions, for vacuum sealing devices, as well as in particle accelerators and surface analyzers. For those applications, properties of many NEG coatings were characterized [4–7]. In physics experiments, they were applied in the Large Electron Positron collider, in the Large Hadron Collider [4], and in general in Synchrotron light machines to minimize the outgassing [8] in form of distributed coatings. They were investigated for the application in the tritium recovery cycles, from early studies (see for instance Ref. [9]) to more recent results [10]. They were tested for the use in tokamaks [9,11,12], and were recently integrated in the limiter of stellarator devices [13]. Vacuum pumps for the HV and UHV regime are often commercialized in combination with ion pumps [2,14,15] having the task of pumping inert gases.

Among active gases that can interact with the getter, hydrogen and its isotopes have a peculiar behaviour, as they are sorbed in a reversible way. In typical conditions, hydrogen dissociates at the material surface, and diffuses in the getter material forming a solid solution. This provides a rather stable pumping speed over time as the bulk of the material contributes to the sorption capacity, not only the surface. A limit to the sorption capacity for NEG elements is exfoliation or hydrogen embrittlement, when subject to cyclic hydrogen loads reaching concentrations above the recommended ones: such effect become less limiting with the introduction of suitable sintering processes in the production of NEG elements. At thermodynamic equilibrium, Sieverts law provides the equilibrium pressure for hydrogenic species as $p_0 = c^2 k(T)$, with a quadratic dependence on the concentration c, and the temperature

* Corresponding author. Consorzio RFX, Corso Stati Uniti 4, 35127, Padova, PD, Italy.
E-mail address: emanuele.sartori@igi.cnr.it (E. Sartori).

https://doi.org/10.1016/j.vacuum.2023.112198
Received 7 February 2023; Received in revised form 13 May 2023; Accepted 15 May 2023
Available online 30 May 2023

dependence expressed by the solubility $k(T)$. Sorption can continue as long as p_0 is significantly below the vessel pressure; in practical applications, the pump will be used to sorb hydrogen until the pumping speed decreases below the required one, or in alternative, a limiting hydrogen concentration is reached. By increasing the NEG temperature, a higher p_0 allows hydrogen removal with auxiliary pumps, to recover the original sorption characteristics for the hydrogen.

The behavior under sorption and regeneration conditions makes the NEG an interesting option for applications requiring hydrogen pumping. However, the operation at relatively high hydrogen pressure and high throughput is not a common application for NEG pumps. The operation with high hydrogen pumping speed, large throughput capacity, and long sorption duration require the development of large pumps: to achieve a good availability, the duration of the hydrogen loading/desorption cycles becomes a strong requirement driving the design, defining the getter mass, the regeneration temperature and auxiliary pumping speed as well as the target pumping speed and operating pressure. In this sense, one of the most challenging vacuum systems is that of neutral beam injectors (NBI) for additional heating in fusion devices. NBIs are an established heating method of many magnetic confinement fusion devices. For heating the core of large fusion plasmas, hydrogen (deuterium) atoms at energies of the order of 1 MeV are required, which can be obtained in NBI from precursors beams of negative hydrogen ions, extracted from a low temperature, caesium-seeded plasma discharge, and accelerated through multi-aperture electrodes [16]. A continuous gas injection is required to sustain the plasma discharge in the ion source; at even larger throughput, gas injection is also required to provide the required gas target density within neutralization gas cells. Such cells have large openings, needed to allow the precursor negative ions to pass through, to be stripped of the electron in the collision with a target gas (see for instance Ref. [17] and references therein). In the optimized ITER NBI design, that can operate with either H_2 or D_2 gas, the injection in the neutralizer requires about ten times larger throughput than in the plasma source [18], totaling more than 40 Pa m^3/s for H_2 (and about 23 Pa m^3/s for D_2) to be sustained for beam pulses up to 1 h. In addition to the required throughput for hydrogen, the target background pressures define, as a consequence, an impressive pumping speed needed. For optimal transmission of the neutralized beam, the lowest possible pressure shall be achieved along the duct connecting the tokamak to the NBI [19]. The vacuum level around the electrostatic accelerator shall remain below 20–30 mPa [20], to minimize stripping at incomplete acceleration of the negative ions that causes beam losses as well as impressive heat loads on the electrodes (up to 2 MW each in the ITER design [21]), but not too low to allow for space-charge compensation of the ion beam [22]. The cryogenic pump designed for the ITER NBI has a target pumping speed of about 5000 m^3/s in H_2 and 3900 m^3/s in D_2 [23,24], a large value, however in line with vacuum system of existing NBI systems (e.g. Ref. [25]). Two (optionally three) injectors will be deployed in ITER, and NBI are also considered for DEMO and fusion power plants given also its ability to provide current good drive efficiency at any radius (see for instance Refs. [26–29]). While on the one hand, alternative schemes for neutralization [30–32] are suggested, to improve the efficiency of this auxiliary heating system but also to mitigate the challenging requirements of the vacuum system, on the other hand research and development on the pumping system is envisaged. The pumping speed stability over time for H_2 of cryopumps (not based on cryo-condensation but physi-sorption), and the fact that a continuous cryosupply at 4 K and 80 K is necessary even when the pump is not pumping, are aspects that limit the availability of NBIs causing relatively frequent regenerations, and decrease further its energy efficiency. Some NEG pumps based on Zr–V–Ti and similar alloys (developed, patented and trade by SAES Getters S.p.A. under the registered trademark ZAO®) [33], are now an appealing option [34] in alternative to cryogenic pumps, and were selected for engineering R&D in view of a possible use in DEMO, within the framework of EUROfusion and the collaboration between Consorzio RFX, Karlsruhe Institute of Technology, and SAES Getters. This paper describes the development path of a NEG pump mockup with a pumping speed of tens of m^3/s, to demonstrate the technology and validate the scaling of its performance to very large pumps such as those needed for NBIs. A modular design has been used, with single getter elements consisting of highly porous sintered disks, arranged in stacks; for this reason, the characterization of the material performances were carried out using setups of increasing dimensions, as discussed in section 2. The pump configuration, which influences the pumping speed as well as the thermal behavior, is presented in section 3. The experimental results of the mockup pump are given in section 4, while being published separately in all details [35]. Finally, in section 5 the perspectives of large NEG pumps for the use in NBI for fusion applications are given, also including practical considerations and ongoing developments.

2. Characterization of ZAO material and small-size ZAO disk assemblies

2.1. Equilibrium pressure

The H_2 equilibrium pressure $p_0(c,T)$ as a function of the hydrogen concentration c for the ZAO alloy was measured in the temperature range T = 300 °C/600 °C [33]. The pressure isotherms provide the temperature and pressure conditions required for regeneration, i.e. hydrogen desorption. Fig. 1 compares ZAO equilibrium to other low-temperature NEG materials suitable for H_2 pumping. The equilibrium curves for the ZAO alloy have the lowest pressure, or in other terms are shifted towards higher concentrations. At temperatures between 500 °C and 600 °C, with a concentration of 650 Pa m^3/kg for example, the ZAO alloy has an equilibrium pressure about four times lower than the St172 and seven/eight times lower than the St707® Getters that are limited for the practical use in fusion applications to a concentration not larger than a few hundreds Pa m^3/kg to avoid the risk of peeling or hydrogen embrittlement. The ZAO alloy was instead successfully tested against fatigue degradation with cyclic loads of hydrogen up to 1850 Pa m^3/kg. The temperature-dependent solubility $k(T)=p_0/c^2$ in Sieverts law is a characteristic of the alloy and of the hydrogen isotope mass, and it is often expressed in exponential form $k(T) = 10^{A-B/T}$, with the constants A, B obtained from the measurement of equilibrium isotherms. Below ~1200 Pa•m^3/kg (i.e. Sieverts region), the equilibrium isotherms for the ZAO can be accurately described by A = 3.64, B = 7290 for H_2 and A = 3.71, B = 7337 for D_2 (with T expressed in K), therefore with a

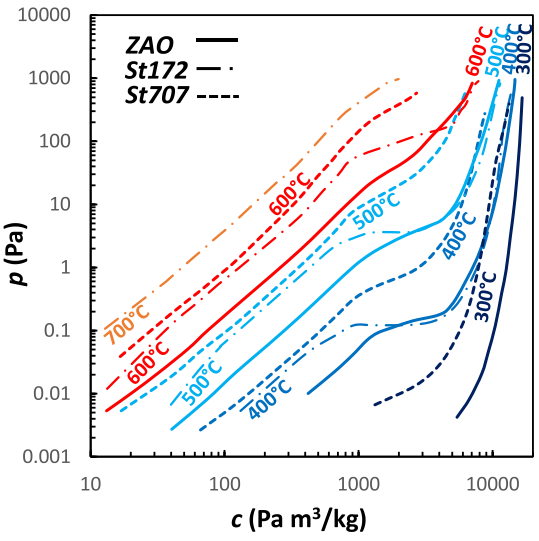

Fig. 1. Hydrogen equilibrium for the ZAO alloy in solid line, in comparison to the Zr–V–Fe alloy (St707) in dotted line, and sintered St172 material in dashed-dotted line.

slightly different solubility for the two hydrogenic species. Such solubility parameters were obtained by fitting the equilibrium temperature in the Sieverts region, as presented in a previous work [34].

2.2. Pumping speed versus concentration and pump geometry

The used ZAO disk has a diameter of 25 mm and a thickness of 2 mm, and the getter mass is 3.5 g. Various methods for determining the pumping speed and sorption capacity were applied in the past, in a standardized manner [36,37] as well as developing a procedure focused on the custom application [38,39]. The initial studies of this work were carried out testing the single disk performances following the ASTM F798-97 [36]. The NEG disk test was carried out as a self-standing sintered getterbody in a UHV system, within a baked chamber of minimal inner surface. The experimental setup of those tests can be seen in Fig. 2. The test is performed by controlling in feedback the pressure in the dosing dome, in order to obtain a stable hydrogen pressure in the test chamber, typically in the 10^{-4} Pa range. The hydrogen throughput Q can be derived from the pressure measured in the dosing dome and in the test chamber, through a well-characterized conductance, and the pumping speed is defined as $S = Q/p$. In this configuration the ZAO disk is not part of a pump, so that the complete surface of the disk is exposed, and it is not hindered by the supporting structure; therefore, it can only provide preliminary indications on the performances to be expected once the disk is part of a pump. In addition, the geometry of the test bench influences the results, as the pressure is measured at a position different from the disk for practical reasons. In numerical simulations presented in Fig. 2, in molecular regime based on Avocado [40], it is found that the measured pressure is about 7–8% higher than the pressure seen by the disk (as shown by the color contours of pressure in the figure); furthermore it is found that the gas load on the two faces of the NEG disk differs by about 6% in this geometric configuration. For a detailed discussion on the general errors that are generally introduced by the ASTM standard measurement the reader can refer to Yoshida [37]. Pumping speeds per unit area $\widetilde{S} = 1/A_N \cdot Q/p$ of the order of 10 m/s were estimated from the measurements, at very low concentrations (i.e. at the beginning of the test) with A_N being the nominal disk surface, somewhat in agreement with independent results obtained by Yoshida for ZAO pills, which are elements of different geometry and different production parameters. A dependence on the pressure for the initial pumping speed at very low concentrations (0.1 Pa m^3/kg) were reported in Ref. [34], for both H_2 and D_2; this dependence is of interest, since NEG are commonly used in UHV regimes, while at tens of mPa the speed for hydrogen decreases by about 30% with respect to UHV.

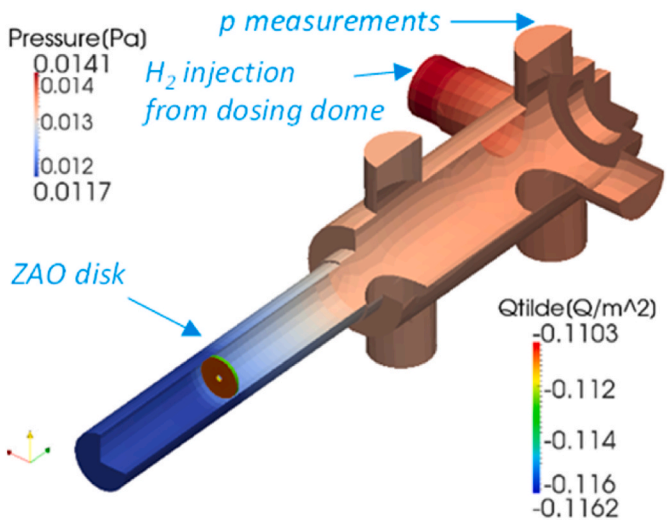

Fig. 2. –Numerical simulation of the gas flow in the test chamber where the NEG disk is placed, reproducing a test at nominal pressure of 13 mPa at the disk position; the color contour shows the hydrogen pressure, at all solid surfaces but the disk, which is colored by specific absorbed throughput $\widetilde{Q}$.

Stacks of disks of progressively larger size were then tested in larger vessels, to better characterize the ZAO performances in configurations more relevant for the final application. Stacks of two sizes, namely 12 and 31 disks, were tested as well as one full cartridge comprising six stacks and totaling about 270 disks, aiming at assessing the interference between the disks when organized in stacks as well as the interference between the disk stacks. The key results in terms of pumping speeds for hydrogen are summarized in Fig. 3. In the following, we will use the subscript *exp* to indicate the effective pumping speed in the vacuum chamber, as derived directly from the experimental measurement of throughput and pressure.

The difference in specific pumping speed $\widetilde{S}_{exp}$ between the 12-disk and the 31-disk pumps depends on the different distance between the disks, which is 0.5 mm in the former and 1 m in the latter setup.

If we intend the thin space between disks in terms of conductance, the influence of such conductance in series to the pumping speed from the NEG surface is more pronounced when the speed is large, at the beginning of the test. Over time, the influence of this effect is reduced and overwhelmed by the reduction of $\widetilde{S}_{exp}$ with concentration. This accounts for the faster speed decrease observed in the case of the 31-disk pump.

The cartridge with six stacks has 1 mm spacing as the 31-disk one, but the stacks shadow each other, resulting a lower specific pumping speed. Anyway, the spacing between the discs is clearly the dominant effect, so that the 270-disk cartridge shows better specific speed than the 12-disk pump.

Finally, the positive effect of the NEG temperature on the speed for hydrogen can be seen by comparing Fig. 3(left) and (right). Sorption tests were considered at room temperature if the getter temperature at the beginning of the test was of ~70 °C or lower. In addition to the expected influence in adsorption kinetics, a higher NEG temperature may reduce the passivating effect of getterable gases other than hydrogen present in the vessel (see section 2.3). At low concentrations, the curve of the 31-disk pump at 150 °C approaches the specific speed

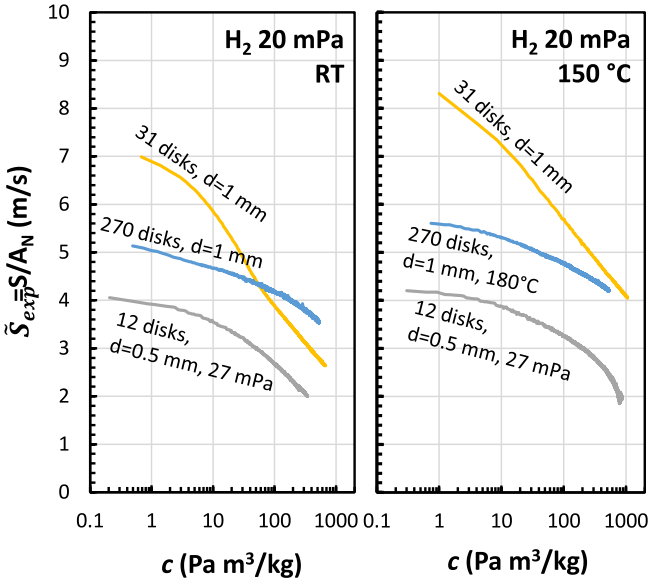

Fig. 3. Sorption characteristics for hydrogen of ZAO disk at RT (on the left) and at 150 °C (on the right), showing the speed per unit area as a function of concentration measured in different setups. Tests on stacks of 12 or 31 disks, and cartridge of 270 disks are reported. Differences between test parameters are indicated in the figure, and discussed in the text.

obtained for the single disks (of the order of 10 m/s as discussed previously). By plotting the pumping speed per unit area for hydrogen as a function of the concentration, we implicitly assume that the speed is a function of state of concentration. Fig. 4 shows the repeatability of absorption runs performed with the 31-disk pump at the same pressure at 150 °C. In this plot, the initial concentration was taken into account and added to the build-up during the test: this explains the different starting point of run #10, which was preceded by an incomplete regeneration. After the relatively fast reduction that occurs at the beginning of the test, the curves overlap for sufficiently high concentration: At 650 Pa m^3/kg, measured total pumping speeds were all within the interval 4.6–5.2 m/s. Within this accuracy, we can state that the conditions of the desorption process (regeneration) immediately before the absorption test did not influence the result. In fact they were all carried out with a different combination of temperatures, in the range 450 °C/650 °C, and durations, from 4 h to 130 h. However, for a pump of new disks the first two (or three) runs generally show progressively increasing performances, indicating the necessity of an initial conditioning for the pump, after which the pumping speed characteristics presents good repeatability. In Fig. 3(a), the 31-disk curve was not preceeded by preparatory runs and might be considered as a lower limit of the stack performance.

It is interesting to discuss the results of numerical models simulating the various disk assemblies, as shown in Fig. 5: large numbers of NEG elements, grouped in recurring patterns, can be studied correlating the pump performance to a pumping speed per unit area of NEG materials (see for instance Ref. [41]). When the pumping condition at c = 1000 Pa m^3/kg is reproduced in the simulations, in the approximation of uniform speed per unit area (i.e. sticking), the specific throughput absorbed at the center of the disks is about 70% of the throughput absorbed at the external cylindrical surface (see for instance the scale of throughput per unit area $\widetilde{Q} = \lim_{A\to 0} Q/A$ in Fig. 5(b)). If we take dS/dc at around 1000 Pa m^3/kg to linearize the pumping speed characteristics, this corresponds to a variation of only 10% of specific speed $\widetilde{S}$. Non-uniformity in the hydrogen load tends to smooth out, as $dS/dc < 0$, but also thanks to hydrogen diffusion within the bulk, contributing to smooth out the difference. Considering that this result is obtained with the small gap of 0.5 mm, and that it is mitigated for larger gaps, we consider not necessary to define a local concentration to study the hydrogen sorption (also quite difficult to account for), and we will treat the experimental sorption characteristics as a mean pumping speed per unit area (or sticking) valid for all surfaces of the NEG.

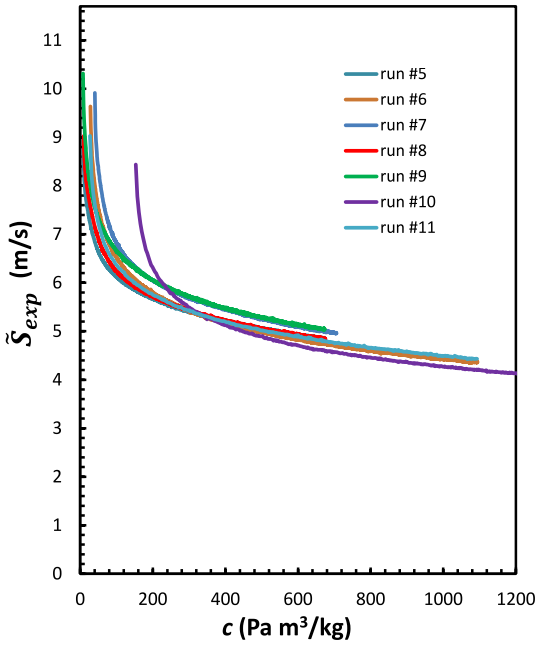

Fig. 4. Repeatability of measured pumping speed for hydrogen as a function of concentration, for various tests of the stack with 31 disks; all absorption tests were carried out at 150 °C.

Numerical simulations were also performed to evaluate the influence of the disk spacing, for the model presented in Fig. 5(c). Aiming at an optimization of the space usage, the total height of the disk stack was kept constant in the investigation, so that the number of disks in the stack was reduced when increasing the spacing. The simulation assumed a fixed $\widetilde{S}$ applied at the disk surfaces, while a total pumping speed $S_{eff} = Q_{sorbed}/p_{chamber}$ was defined as it would be measured in the experiment (i.e. analogous to S_{exp}). Interestingly enough, an almost constant total pumping speed S_{eff} was found for a spacing between 0.5 mm and 1 mm; the apparent pumping speed per unit area $\widetilde{S}_{eff}$ increases, inversely with the number of disks as detailed in Table 1, even though the total pumping speed of the stack increases with the number of disks. It is important to notice that the uniformity of gas load rapidly decreases when the spacing decreases below 1 mm, with only minor improvements above. The effect of increasing the transparency of the stack on the effectiveness of heating via radiation will be discussed later.

The uniformity of gas load during the sorption phase was studied in detail with numerical simulations of the six-stack cartridge with spacing of 1 mm [42]. It was shown that the effect of the external cage on both the pumping speed and the uniformity of gas load is negligible, and in general it does not influence the pumping speed (with a reduction between 7% and 5%). The uniformity over the disk planar surface is within 16% from the outer side to the inner side, while the cylindrical faces were found to have about 40% less gas throughput on the inner side. The contribution of porosity and bulk diffusion was not discussed. Due to the complexity of an accurate modelling of every single NEG disk in large pump assemblies, the authors discussed possible simplifications of the geometry, including modelling the stacks as full cylinders or just reducing the cartridge to a prism of hexagonal base. The authors report a total pumping speed of 1.08 m^3/s on the NEG disk surfaces at c = 400 Pa m^3/kg. From those results, we can calculate $\widetilde{S}$ = 4.2 m/s at the disks when considering the number of disks and their exposed area, while the pumping speed per unit area that would be derived converting directly the measured speed is $\widetilde{S}_{eff}$ = 3.3 m/s. The ratio is $\widetilde{S}/\widetilde{S}_{eff} \approx 1.3$, while for the single stack it is about 1.1. These results are somewhat consistent with the difference shown by experimental results of Fig. 3(b). Therefore a coefficient $d_{cartr} = \widetilde{S}_{eff}/\widetilde{S} = 0.77$ accounting for this cartridge geometry can be introduced. It was shown that, in order to reproduce the experimental results in terms of gas throughput and vessel pressure at three concentrations along the sorption curves, the pumping speed per unit area to be assigned to the simplified geometries does not keep the same ratio with respect to the specific speed to be applied when each disk is modelled. In particular for the hexagonal case, the variation is within ± 3.5%; if accuracy within this range is acceptable, large NEG pumps composed of cartridges can be modelled by hexagonal boxes, with large improvement of the computational cost.

2.3. Other aspects influencing the pumping speed: pressure, isotope, co-adsorption of other species and venting

An approximate relation describing the relative reduction of the speed for hydrogen on the operating pressure p with respect to a reference value provided at p_0 is

$$d_p = \frac{\delta - \xi \ln(p)}{\delta - \xi \ln(p_0)} \qquad \text{eq. 1}$$

The coefficients δ and ξ, only valid around certain concentrations c_i, are proposed in Table 2. At low concentration, of the order of 0.1 Pa m^3/kg up to 10 Pa m^3/kg, (also confirmed by the results of the large mockup within the range 10 mPa–100 mPa) the speed decreases with increasing

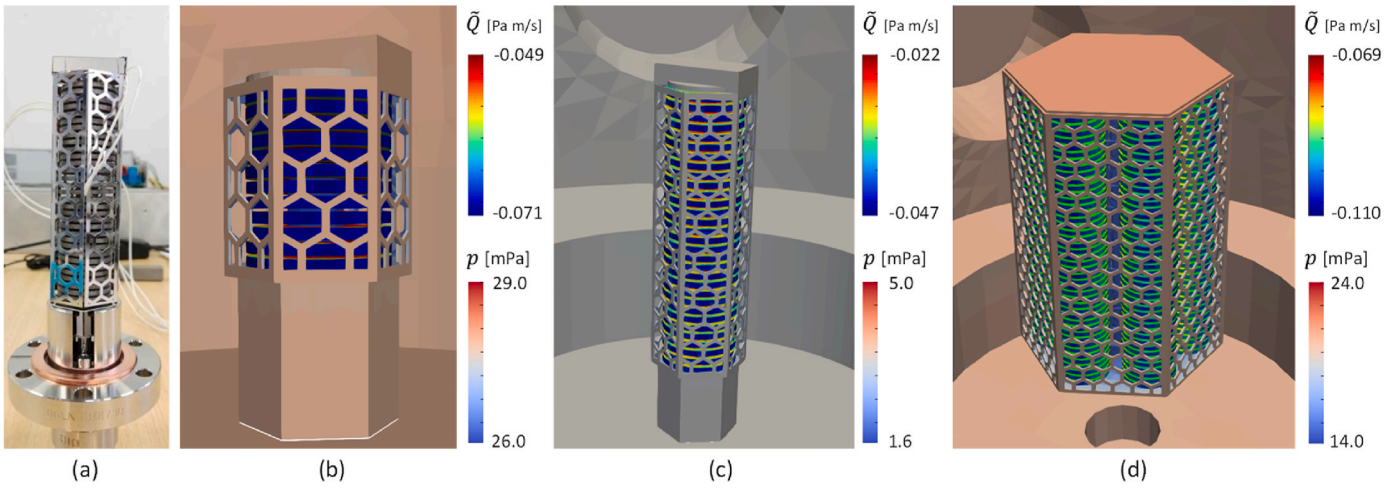

Fig. 5. (a) picture of the stack with 31 disks, spaced 1 mm; (b), (c), (d) Examples of numerical simulations of the different configurations: from left to right, 12 small disk stacks, 31 disk stack (for which different disk spacing was also simulated), 270 disks cartridge. For all simulation results, getter disks are colored by throughput per unit area, while the other surfaces are colored by pressure contour.

Table 1
Effect of disk spacing in terms of total pumping speed S, pumping speed per disk S/N, and effective pumping speed per unit area $\tilde{S}_{eff}$ obtained for a disk stack of constant height (about 92 mm).

Disk spacing	*N of* disks	S_{eff} (m^3/s)	S_{eff}/N (L/s)	$\tilde{S}_{eff}$ (m/s)
0.5 mm	36	0.082	2.29	2.32
1 mm	31	0.082	2.65	2.68
1.5 mm	26	0.072	2.76	2.79
2 mm	23	0.065	2.81	2.84

Table 2
Coefficients for pressure dependence at room temperature.

c_i	0.1–10 Pa m^3/kg	500 Pa m^3/kg
δ	0.00294	0.463
ξ	0.167	0.178

pressure. However, at higher concentrations, the dependence on pressure appears to flatten out or even to invert its behavior.

NEG pumps are capture pumps based on sticking of gas particles on the adsorption sites of a surface; for a given sticking probability, its pumping speed depends on the impingement rate, which depends on the thermal velocity and therefore on the square root of the particle mass. In principle, the chemical reactivity of hydrogenic gases H_2, D_2 does not depend on the isotope mass. In such limit conditions, the pumping speed for deuterium shall be $\sqrt{2}$ lower than for hydrogen; however, the diffusion coefficient from the surface into the bulk material of the dissociated atom depends on its mass, and this effect might contribute on the total pumping speed. The experimental results on the isotope effect will be discussed in section 4, including results of the mockup pump.

The influence of the absorption of other active gases on the hydrogen pumping speed of ZAO disks was also studied. It was shown [43] that, in approximate terms, the relative reduction in speed for hydrogen is proportional to the reduction of active sites caused by the adsorption of N, O, C species chemically bonded on the getter surface. At low getter temperatures, the surface saturates without diffusion of these species in the bulk, and the surface is not renewed until the getter is heated. To quantify the effect of air constituents and carbon oxides, Fig. 6 shows the pumping speed for the i-th species per unit area $\tilde{S}_{exp,i}$ versus the absorbed quantity per getter area $\sigma_{BG,i}$, at room temperature. The capacity was

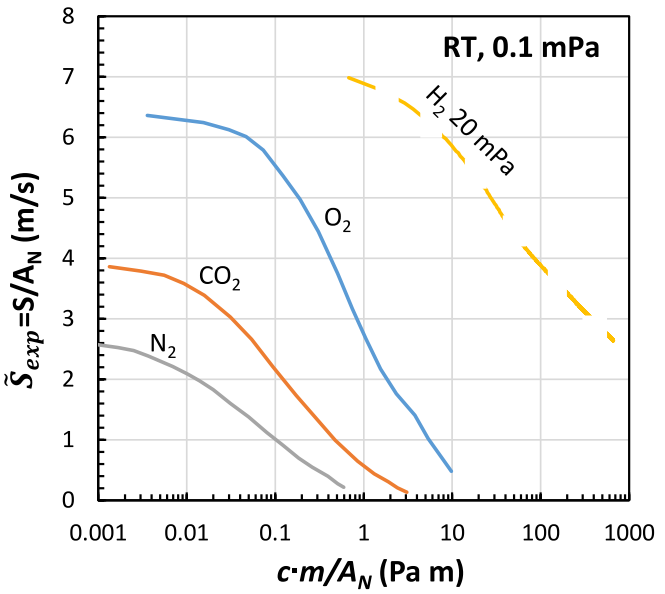

Fig. 6. Pumping speed per unit area for nitrogen, oxygen and carbon dioxide [43] at room temperature obtained with a stack of 31 disks. The pumping curve for hydrogen is included for comparison.

found to be about five times larger already at 150 °C. In a vacuum vessel with outgassing rate of impurities $Q_{out,i}$ for the i-th specie, the relative decrease of hydrogen pumping speed with respect to the initial value $d_i = \tilde{S}_{exp,i}(\sigma_{BG,i})/\tilde{S}_{exp,i\,0}$ would depend on the absorbed quantity per unit area $\sigma_{BG,i}$ of getterable background gases:

$$\sigma_{BG,i}(t) = \sigma_{BG,i}(t_0) + p_{BG,i}\int_{t_0}^{t} \tilde{S}_{exp,i}dt \approx \tilde{Q}_{out,i}t \qquad \text{eq. 2}$$

We propose an approximate relation describing the relative decrease over time of the speed for hydrogen

$$d_i = \alpha_i - \beta_i \ln\left(\tilde{Q}_{out,i}t + \gamma_i\right) \qquad \text{eq. 3}$$

to be determined from the single contributions of outgassing per getter unit area $\tilde{Q}_{out,i}$, with the coefficients given in Table 3. The effect of water adsorption on the speed for hydrogen could be considered similar

Table 3
Coefficients for eq. (3) at room temperature.

	N_2	O_2	CO/CO_2
α	0.00294	0.463	0.177
β	0.167	0.178	0.161
γ	0.0025	0.048	0.006

to that of O_2, within a factor two on the absorbed quantity according to the stoichiometric ratio. As said, an increase by a factor five on the maximum concentration of co-adsorbed species would apply if the NEG is maintained at 150 °C; this can be easily included in eq. (3) by reducing the specific throughput $\widetilde{Q}_{out,i}$ by the same factor. The discussion of hydrocarbon pumping is also given in Ref. [43].

Experiments on stacks of 45 ZAO disks were carried out to quantify the effect of venting. The two series of tests presented in Fig. 7 were carried out following two different protocols. In the first case, the hydrogen absorption tests of the shortest duration were done, followed by a CO adsorption test until surface saturation, and venting was carried out with N_2 gas. In the second protocol, the presented pumping speed is defined at 133 Pa m^3/kg of concentration, no CO test was carried out, and venting is performed directly in air. Despite the different protocol, the effect of venting on the ZAO disks was quite the same; furthermore, in both cases, by increasing the duration of reactivation (marked with the arrows in figure), the initial pumping speed for hydrogen was fully recovered (or increased). In the scenario of NBI applications, the number of exposures to air can be quite small, while it can be larger in the case of NBI test facilities.

2.4. Regeneration

The influence of temperature and auxiliary pumping speed on the regeneration phase was experimentally tested on the prototype stacks, as reported in Ref. [33], and on the one-to-one cartridge prototype. It was verified that, in static conditions, the initial hydrogen concentration c_i could be obtained from Sieverts law in pumps of arbitrary dimensions, as $c_i = \sqrt{p_i/k(T_{reg})}$. It should be noted that a certain time is required to reach a steady-state regeneration temperature T_{reg}, and that slower heating ramps are applied to large pumps to avoid local overheating and thermal stresses. Therefore, the NEG material has time enough to balance uneven gas loads, and getter parts at different concentrations evolve along the equilibrium curves towards an average condition. For this reason, the equilibrium pressure reached at steady state represents not only an effective average, but an instantaneous equilibrium (even though different from the hydrogen load distribution when heating was started). A unique equilibrium pressure applies to the whole getter material, so that in the presence of temperature non-uniformities, the getter evolves along different isotherms, reaching slightly different concentrations, as $c'/c = 10^{0.5B(1/T'-1/T)}$. For instance, in a regeneration at 600 °C, ZAO material at 560 °C will have a 60% higher concentration (when within the Sieverts region). Achieving a temperature as uniform as possible is therefore an important criteria for the thermal design of a NEG pump; on the other hand, non-uniformities cannot be avoided, and the concept of effective temperature can be introduced to model the pump behavior even if the getter temperature is known only at one position. By delaying the application of auxiliary pumping, after steady temperatures are reached, the initial equilibrium pressure p_i can be measured at the beginning of regeneration; similarly, p_f can be measured by insulating the vessel from the auxiliary pump at the end of regeneration. A better estimation of the initial and final concentration c_i and c_f can be obtained in this manner.

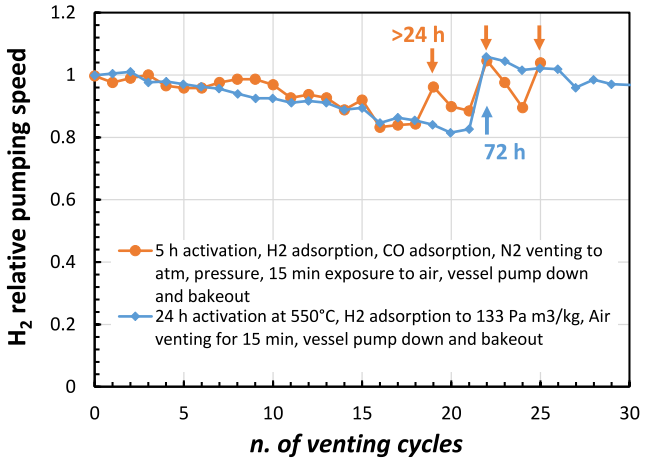

Fig. 7. Pumping speed for hydrogen, repeatedly measured after exposure to air and subsequent activations, with two different protocols: the same regeneration temperature of 550 °C was applied in both cases.

Characterizing in advance the effective pumping speed versus vessel pressure $S_{aux}(p)$ of the pumping speed applied during regeneration (i.e. auxiliary pumping) allows calculating the reduction of concentration over time, from the measured pressure. The concentration varies over time as

$$c(t) = c_i - \frac{1}{m}\int_0^t pS_{aux}(p)dt, \qquad \text{eq. 4}$$

to be solved via numerical integration. Under equilibrium conditions, i.e. no temperature transient and no limitation from bulk diffusion of hydrogen, Sieverts law $p = c^2k(T)$ can be combined with the effect of auxiliary pumps, to describe the mean variation of concentration c over time:

$$\frac{dc}{dt} = -\frac{c^2k(T)}{m}S_{aux} \qquad \text{eq. 5}$$

with m the getter mass. The particular solution of the first-order differential eq. (5),

$$1/c = S_{aux}k(T)/m{\cdot}t + \text{const} \qquad \text{eq. 6}$$

indicates that by plotting the inverse of the average concentration derived from experimental tests over time, and obtaining the slope of the curve, an effective regeneration temperature T can be derived, as long as S_{aux} is constant and the relation $k(T)$ is known from the isotherms. As an example, Fig. 8(b) presents the concentration over time obtained from p (t) following eq. (4), for two regenerations of the 31-disk stack at 550 °C with 5.5 L/s and 139 L/s respectively. Fig. 8(a) shows the linear relation of eq. (6). As shown in Fig. 8(b), the regeneration curve directly obtained from the instantaneous pressure measurements (black lines) is well reproduced when the results of the linear regression are considered (red lines), but only when T and S_{aux} are constant coefficients, which is not the case for the initial part of the dashed line. In general, the early part of the regeneration shall not be included in the linear regression, because the NEG temperature might not be at steady state, and not quite uniform for the NEG material; in addition, because of the high initial concentration, the equilibrium pressure might reach a relatively high value so that the auxiliary pump operates at reduced speed. If a precise quantification of the concentration c_i at the beginning of regeneration is required, the NEG pump could be heated until steady conditions without auxiliary pumping; as said, the average concentration could be obtained from the equilibrium pressure reached in these conditions. However, in case of low regeneration temperatures or low concentrations, the partial pressure of non-getterable gases could influence the measurement, and the equilibrium pressure could be obtained only after the auxiliary pump starts. Estimating c_f at the end of regeneration by closing the auxiliary pumping is straightforward; when dealing with large NEG pumps (i.e. the auxiliary pump has a much lower speed than the NEG pump), the vessel pressure equals the equilibrium pressure already under auxiliary

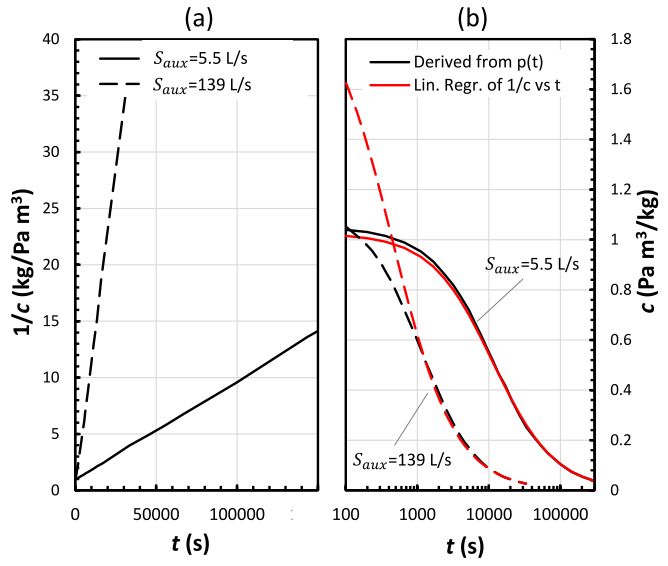

Fig. 8. Analysis of two regenerations of the 31 disk stack, at the same nominal temperature 550 °C, but two different auxiliary pumping speeds as indicated in the legend. (a) linear regression as obtained from the concentration over time; (b) curve of concentration versus time derived from the direct measurement of instantaneous pressure (in black), and "synthetic" curve reconstructed from the parameters of the linear regression (in red).

pumping. By substituting $k(T)$ in eq. (6), integrating over time the concentration and reversing, the regeneration duration reads [3]

$$t = \frac{m}{S_{aux}}\left(\frac{1}{c_f} - \frac{1}{c_i}\right) 10^{-A+B/T} \qquad \text{eq. 7}$$

This solution is strictly valid as long as S_{aux} is constant, a condition that might not be verified experimentally: this is the case for instance of turbopumps when, at the beginning of regeneration, an equilibrium pressure of the order of few Pa might be reached.

3. Configuration of the modular mockup pump

As said, constructing and testing a mock-up pump of significant dimensions is a fundamental step in the technological development of large-scale NEG pumps for the application to nuclear fusion devices. As discussed previously, scaling of NEG performances for hydrogen was studied experimentally testing ZAO pumps of increasing dimensions. Experimental tests had to cover also the reliability of components during all phases of operation, also including thermal characterization of disk assemblies of different configurations.

The three pump concepts presented in Fig. 9 based on sintered ZAO

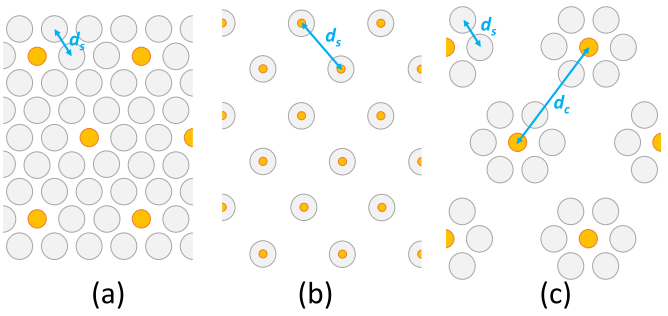

Fig. 9. Three configurations studied during the conceptual design. Colored circles represent heaters.

disks were identified and studied [44], following the main criteria detailed in the following.

The uniformity of the heating scheme and its reliability are of great importance. In the case non-uniform heating is applied during activation or regeneration, a certain fraction of the NEG material might follow a completely different gas loading cycle. For instance, a higher value of hydrogen concentration could be reached risking embrittlement, or the surface of some disks might not be properly reactivated after chemisorption of impurities, affecting the pumping speed for hydrogen. Another essential requirement is a high availability of the pump. In this sense, limiting as much as possible the duration of the cooling down phase can be essential to minimize the duration of the regeneration cycle, depending on the specific application. Finally, the efficiency of the heating scheme also plays a role. The total power required for regeneration should be minimized, exploiting mutual irradiation between the stacks of discs to keep the heating power per getter mass smaller than that of single-stack pumps, with disk spacing of 1 mm, of the order of 0.4 kW/kg. On the other hand, a reliable heater design is easier to achieve when the nominal power is maintained as low as possible. From the point of view of maintainability of the pump, a modular design that minimizes the number of heaters, electrical connections and feedthroughs is to be preferred. More quantitative criteria are the pumping speed, and the getter mass, per unit volume; these indicators are quite important, as the cost and complexity of a fusion facility generally scales with the volume of the vacuum vessel.

Practical engineering constraints were also taken into account. Among others, the longitudinal extent of heaters is limited. They are composed by tungsten or tantalum wire, wrapped in some fashion about an alumina tube or screw; based on the SAES experience in commercial pumps the length was limited to about less than 150 mm, because of relative thermal deformations, and of the voltage drop at the filaments. A practical limit concerning the height of the stack of disks was also considered, due to assembly issues (handling during assembly, tolerances given by many disks and spacers), as well as mechanical aspects. A shorter and stiffer assembly is to be preferred, for the vibration modes and seismic loads to be verified for the use in nuclear environments. A grid with large transparency F around the disks stacks was considered as well, to provide a rigid mechanical structure supporting the stacks. At the first order, the influence on the pumping speed of such grids can be calculated as a conductance in series with the stacks. Per unit area of exposed NEG disks, the conductance in series reads $\tilde{C}_{grid} = 0.25\, v_{th} F \cdot A_{grid}/A_{NEG}$, with v_{th} the average thermal velocity of H_2 molecules. With $F = 0.5$ at room temperature, for the case of single stacks we have $A_{grid}/A_{NEG} \approx 1/5$ and $\tilde{C}_{grid} \approx 40$ m/s, while for the case of the cartridge we have $A_{grid}/A_{NEG} \approx 1/18$ and $\tilde{C}_{grid} \approx 12$ m/s. Both specific conductances have a small impact on the specific pumping speed of the NEG. On the other hand, as discussed in Ref. [44], the presence of a grid with $F = 0.5$ around the getter disk halves the heat dissipation, acting as an intermediate screen for radiation.

As detailed in Ref. [44], molecular flow simulations were carried out for the mockup pump configuration, by simplifying the disk stacks to cylinders of effective pumping speed. The pumping speed per getter mass, the uniformity of the gas load, and the gross dimensions of the mockup pump are reported in Table 4. The uniformity is given as the ratio of the lowest to the highest specific throughput calculated along the cylinders of disks. Due to the non-uniform gas load, to avoid overcoming a limit on hydrogen concentration in the most loaded parts of the pump, a reduced hydrogen capacity would be available; the table provides a rough estimation as if a rather low limit of c = 660 Pa m^3/kg was defined. The pumping speed per unit mass and the pumping speed per unit volume indicate that the concept of Fig. 9(a) could be advantageous if a small volume is available, but the uniformity of gas load would be unacceptable; concept (b) and (c) are similar. In the same manner, the NEG temperature evolution in the heating and cool down phases were also calculated. When simulating getter regeneration and applying the

Table 4
Dimensions and calculated pump performances for the three concepts shown in Fig. 9.

Config.	*m* (kg)	d_s, d_c *(m)*	*H, L, W* (m)	V (m^3)	S (m^3/s)	S/m (m^3/(kg•s))	S/V (1/s)	Unif.	*Gas capacity (Pa m^3)*
(a)	32.0	0.03, -	0.134, 0.57,0.33	0.025	20.7	0.65	828	16%	*12300*
(b)	31.2	0.062, -	0.3, 0.91,0.31	0.085	36.6	1.17	430	84%	*18900*
(c)	32.1	0.03,0.18	0.3, 0.98, 0.39	0.114	35.1	1.09	307	77%	*18700*

same heater temperature, configuration (a) offered a rather poor temperature uniformity at steady state ($T_{min}/T_{max} = 0.59$) in comparison to configuration (c) that used the same heating scheme ($T_{min}/T_{max} = 0.79$). Thermal simulations clearly indicated that a different heating power should be applied for the tests, possibly grouping the heaters depending on their position within the pump, in order to obtain a uniform temperature for the NEG disks. Thermal simulations of the cartridge indicate non-uniform temperatures of the disks, but also a variation along the disk stacks (with 40 °C less at the edges, for nominal regeneration temperature of 550 °C); these results, obtained in simplified geometry and affected by uncertainties on the surface emissivity of the various elements, confirmed the importance of deriving an effective getter temperature from the regeneration tests. Under simplifying approximations, configuration (a) showed also a neat difference in characteristic time for cooling down (longer by a factor of two at the least), with the central stacks having a much slower temperature decrease than those on the outer sides of the mockup. Configuration (c) was preferred to configuration (b), as it offered less complexity of electrical connections, less heaters that could also integrate a redundant circuit, simpler assembly, installation and maintenance, because it groups six stacks of disks and one heater into single independent cartridges.

Cartridges with six stacks of 45 disks in hexagonal configuration with $d_s = 0.03$ m, $d_c = 0.18$ m were constructed. Multi-bore alumina tubes with tantalum filament were selected as heaters, located at the center of the cartridge. A rigid cage encloses the disk stacks with a transparency of 0.5. A sandwich structure, partially transparent to gas flow, was realized as a support for the cartridges mounted on both sides, up to a total of 34 cartridges, and to house the cabling inside. Electrical connections were realized with bare copper cables insulated with alumina tubes and beads. The cartridges were grouped in five sections depending on their positon, and one single temperature reference was taken for each group, to control in feedback the regeneration temperature (the division in sections is illustrated below in Fig. 16). With a master-slave concept, the cartridges can be operated with identical electrical parameters within each of the five sections. This concept can be scaled to larger configurations. The thermocouple used for controlling the heating power was installed inside the tube on the axis of a disk stack. Several other thermocouples were installed on different positions at the pump: directly on the NEG disks, on the support structure, on the cartridge cage. The AISI 304L sandwich structure, about 1 m long and 0.5 high, can be mounted on a rigid support frame, possibly to be connected to the vessel flange. The tests were to be carried out on the TIMO facility [45]: given the design of the facility, it was decided to connect the frame to the large flange that closes the vessel. Modal analyses indicate that the sandwich structure has a minimum resonant frequency of 96 Hz, for an out-of-plane deformation mode (i.e. direction parallel to cartridge axes) with a 40% mass participation fraction. The response spectra of cartridges along the vertical direction is found at a much higher frequency (152 Hz). As a comparison term, the first resonant frequency is sufficiently high with respect to the response spectra expected for seismic loads in the case of the ITER building (with peak below 10 Hz). The threaded connections of stainless-steel cartridges were realized in Nickel Aluminium Bronze to avoid in-vacuum bonding at high temperature. Sockets offering the electrical connection were designed to allow connecting the cartridges with good accessibility; a manual procedure for fixing the connections was required. Fig. 10 shows the assembled mockup pump with 17 cartridges installed all on one side of the sandwich structure, ready for the test in TIMO. After an initial phase of tests, the design was revised and improved as discussed at the end of the following section.

Fig. 10. Picture of mockup pump fully assembled with 17 cartridges.

4. Results of mockup pump characterization: measurements and analyses

The TIMO facility was used for testing large cryogenic pumps for ITER; it has a hydrogen inventory certification up to 20 mol, an inner volume of 10 m^3 in a cylindrical vessel about 1.7 m in diameter. The developed NEG pump was tested in TIMO extensively [35], and the main results are discussed in the following.

4.1. Pumping speed

The speed for hydrogen per getter unit area measured for the mockup pump is presented in Fig. 11, for sorption tests at room temperature and at 180 °C. The tests were carried out at constant gas throughputs. The total pumping speed S_{exp} was calculated from the instantaneous vessel pressure p and the injected throughput Q, as $S_{exp} = Q/p - S_{TMP}$. The pressure reported in figure is the one obtained at the beginning of the test: it steadily increases over time as the pumping speed decrease. At 650 Pa m^3/kg, the specific speed at RT is around $\widetilde{S}_{exp} = 3.1$ m/s, not much lower than $\widetilde{S}_{exp} = 3.5$ m/s at 180 °C. The pumping speeds per unit area are therefore in line with the characterization of the smaller disk assemblies. For instance, the specific speed for hydrogen of the single cartridge at 140 °C (conveniently shown, together with mockup results, in Fig. 11 as dashed grey line) is about 0.5 m/s above the speed per unit area derived for the mockup sorption curve at 180 °C. The specific speeds discussed before correspond to a pumping speed of the mockup of 13.6 and 14.8 m^3/s respectively for RT and 180 °C operation (0.8 m^3/s and 0.87 m^3/s per cartridge), while the concentration of 650 Pa m^3/kg corresponds to 10.5 Pa m^3 of gas load. The effective pumping speed for hydrogen of the turbopump $S_{TMP}(p)$ was experimentally characterized in advance. The characterisation was extended to 2.1 Pa, a pressure at which the turbopump speed is reduced to 30% of the nominal value, in order to permit the quantification of the desorbed hydrogen amount

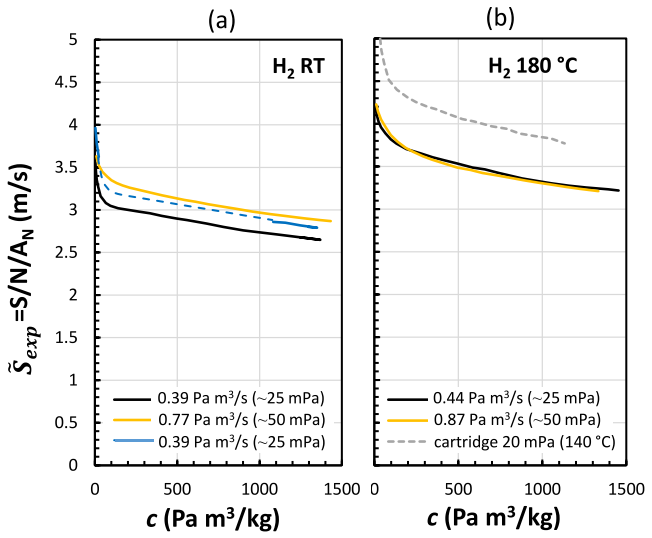

Fig. 11. Measured pumping speed per unit area for the mockup pump, in hydrogen. The left panel shows results of the test at room temperature with constant H_2 throughputs: the resulting vessel pressure at the beginning of the test is also indicated. The blue curve in the left plot presents the incomplete data of one test; the dashed line that complete the curve is just a guide for the eyes. The right panel presents results of constant throughput tests at 180 °C, providing initial vessel pressure as of the tests at RT. The dashed grey line is the measured speed of one single cartridge in a constant-pressure test at 140 °C.

during regenerations.

As for the 31 disk pump, repeatability and consistency of the pumping speed measurements when plotted as a function of the concentration was confirmed.

As the pumping speed can be considered a function of state of the concentration, a practical formula describing the pumping speed as a function of c can be derived. The formula shall reproduce the quasi-linear decrease of speed at concentrations, 100 Pa m^3/kg after the starting concentration. A convenient expression for NEG pumps (only valid for cartridges of ZAO disks with this specific arrangement) is

$$\widetilde{S}_{exp}(c) = \eta \exp(-\psi(c - c_0)) - \mu c + \widetilde{S}_{exp\,0} \qquad \text{eq. 8}$$

where $\widetilde{S}_{exp\,0}$ is the intercept at zero concentration of the linearised part of the pumping curve. The first term on the right hand side accounts for the rapidly-decreasing speed at the beginning of the sorption phase: coherently with results of Fig. 4, it was defined as a function of the initial concentration c_0. The parameters given in Table 5 reproduce with good accuracy the curves of Fig. 11 up to 1300 Pa m^3/kg.

In general, the pumping curves for deuterium show trends similar to those for hydrogen. At 180 °C, the pumping speed curves for deuterium overlaps those for hydrogen if the square root of mass ratio is used to reduce the speed, but also the concentration: the small differences are highlighted in Fig. 12, in which the sorption curves of the mockup pump are presented after correcting both the specific pumping speed and the concentration with the square root of the molecular mass M of the hydrogenic specie. It is possible that the different dependence on concentration by the two molecules is somewhat correlated to the different

Table 5
Coefficients for eq. (8) at room temperature.

	RT	180 °C
$\widetilde{S}_{exp\,0}$ (m/s)	3.07	3.75
η (m/s)	0.5	0.46
ψ	0.038	0.015
μ (kg s^{-1}Pa^{-1}m^{-2})	0.00032	0.0004

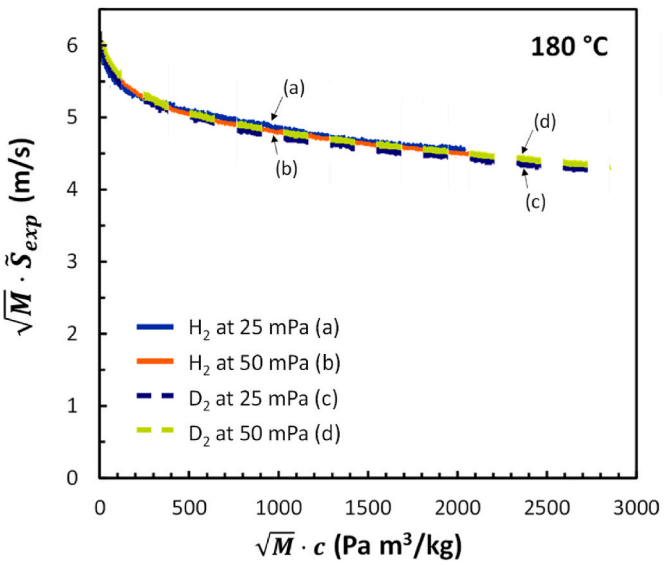

Fig. 12. curves of pumping speed versus concentration for hydrogen (solid) and deuterium (dashed lines) at 180 °C, corrected with the square root of the molecular mass M given in atomic mass units.

solubility $k(T)$, discussed in section 2.1, that is found for H_2 and D_2. It must be noted however that the slope of the curve $\widetilde{S}_{exp}(c)$ is small, so that correcting the pumping speed only (i.e. only the y axis) might be accurate enough for most practical uses at low concentrations. A less clear behavior is found at room temperature: Fig. 13 compares the pumping speed for different concentrations and sorption pressures, presenting together results of the single ZAO disks and of the mockup pump. Ratios, calculated using the pumping speeds at identical concentrations for the two species, are spread around the square root of mass ratio, and they are lower than that in all cases but one.

For these evidences a correction coefficient d_M for the pumping speed that accounts for the isotope mass is suggested, with recommended values $d_M = 1$ for H_2 and 0.71 for D_2. It could be speculated that, to improve the phenomenological description, also the concentration c in eq. (8) shall be corrected by $1/d_M$; however this is debatable and shall be further investigated experimentally, or justified by a physical model.

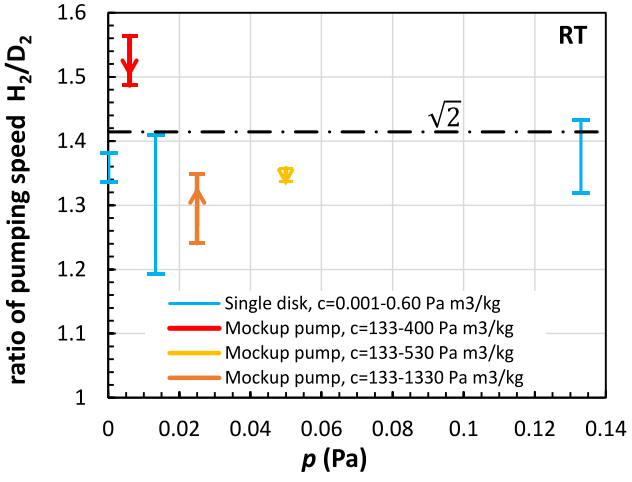

Fig. 13. Ratio of pumping speed for hydrogen and deuterium at room temperature, for various absorption pressures and concentrations. Ratios vary with the concentration, as indicated by the vertical extent of the bars; arrows indicate the orientation from low to high concentration. Note that the points from the mockup tests, measured with a capacitive gauge, at p < 0.01 Pa are affected by an error at least ten times larger than those at high pressure p = 0.1 Pa.

4.2. Simulations

The sorption tests in TIMO were also simulated in molecular flow regime [40], an approximation that is marginally applicable for this system, having a Knudsen number of the order of 0.4 at a pressure of 20 mPa when the diameter is taken as characteristic length. Fig. 14(a) presents the TIMO geometry with the installed mock-up: all surfaces are colored by H_2 pressure, but the lateral surfaces of the NEG cartridges, having an overall surface of 0.765 m^2, which are colored by throughput per unit surface $\widetilde{Q}$. The simulation parameters were tuned to reproduce a test at 180 °C, with injected H_2 throughput of $Q = 0.487$ Pa m^3/s (yielding an initial pressure of 25 mPa); in particular at a concentration of 650 Pa m^3/kg, the measured vessel pressure is 28.9 mPa so that the experimental estimation of the pumping speed is about 15.3 m^3/s. The specific pumping speed $\widetilde{S}_{hex} = 22.0$ m/s was applied at the surface of the cartridges (total applied $S_{hex} = 16.83$ m^3/s), resulting in a vessel pressure at the gauge position of 28.9 mPa. The corresponding capture coefficient at the six lateral faces of each cartridge reads $s = 4\widetilde{S}_{hex}\sqrt{\pi M_{H_2}/8k_BT} \sim 0.05$, with M_{H_2} the mass of the H_2. Because of either the geometrical configuration of the test, or the configuration of the NEG pump, the installed pumping speed per cartridge of $S = 0.99$ m^3/s was higher than the value that can be obtained from direct conversion of the experimental measurement $S_{exp} = 0.90$ m^3/s. In large NEG pumps based on multiple cartridges with this arrangement a decrease factor d_{multi} of the order of 0.9 might be considered to account for the lower effective speed with respect to the installed one; however, dedicated simulations shall be carried out to deal with specific geometries. The contribution from the turbomolecular pump was also included in the simulation, performing a dedicated calculation without the NEG pump; the experimental characterisation of the turbopump could be replicated by applying a speed of 1.72 m^3/s at the surface indicated in Fig. 14(a).

The uniformity of the gas load is discussed in Fig. 14(b). The gas throughput at four cartridges was calculated by integrating the specific throughput at their open surfaces, and the variation in percentage with respect to the average is indicated in the figure. As expected the external cartridges and in particular the ones installed towards the gas injection receives a higher gas load, meaning that all cartridges contribute in a rather equivalent amount to the total pumping speed. In a simulation reproducing the conditions at slightly higher experimental pumping speed of 18 m^3/s, and at lower pressure of 14 mPa, the relative variation of gas load is more pronounced, as the central cartridge receives 96.3% of the average load, and the corner one 103.6%. Therefore, in large NEG pumps with modular design based on cartridges, the non-uniformity of gas load depends on the instantaneous pumping speed and operating pressure, but according to these calculations, the spacing between cartridges (face-to-face distance of about 100 mm) is enough to limit the non-uniformity within ±3.6% form the average.

As a final result, let us discuss the average specific pumping speed $\widetilde{S}$ at the surface of the disks. This can be achieved by combining the decrease factor $d_{multi} = 0.9$ quantified previously for the mockup, with the detailed simulation of one cartridge discussed in section 2.2, which provided $d_{cartr} \approx 0.77$ (for values of $\widetilde{S}_{eff}$ similar to $\widetilde{S}_{exp}$ measured during the mockup test). In summary, numerical simulations can be used to derive the pumping speed per disk area $\widetilde{S}$ from the effective one derived experimentally, given in eq. (8), and

$$\widetilde{S}(c) = \widetilde{S}_{exp}(d_{cartr}d_{multi})^{-1}, \qquad \text{eq. 9}$$

yielding $\widetilde{S} \approx 1.45 \cdot \widetilde{S}_{exp}(c)$ for this pump design. In correspondence of $\widetilde{S}_{exp} = 3.5$ m/s at a concentration of 650 Pa m^3/kg with 180 °C, we obtain $\widetilde{S} = 4.9$ m/s, or in other terms a sticking factor of about 0.011 (which reduces to 0.0099 at RT). These values of sticking factor are in line with the literature (see for instance the recent review by Yoshida [37]).

4.3. Regeneration

The instantaneous hydrogen throughput $Q(t)$ desorbed from the NEG during regeneration is calculated from the measured vessel pressure $p(t)$ and the auxiliary pump characteristics $S_{aux}(p)$. The average concentration evolves as $c = c_i - 1/m \int_0^t Q \cdot dt$. The analysis of three regenerations, carried out at different nominal temperatures, is presented in Fig. 15, in form of inverse concentration $1/c$. The linear part represents a condition of steady-state temperature, and pressure below 2 Pa for each of the three regenerations (a condition for which the turbopump speed is constant, $S_{aux}(p) = 1.65$ m^3/s). The effective temperatures that justify these slopes are reported Table 6. The slope $a(T_{eff}) = S_{aux}k(T_{eff})/m$ is obtained from linear regression $1/c = at + b$, and the effective temperature is obtained as $T_{eff} = -B/\log_{10}(k \cdot 10^{-A})$. The analysis shows that the effective temperature is about 1% less than the nominal temperature: this means that thermocouples inserted inside the tubes constituting the axis of disk stacks are a good indicator of the effective regeneration temperature, and can be used as feedback for the power supplies during regeneration. In addition, this is a further confirmation that the thermal behavior was rather homogeneous within each of the sections identified for the master-slave control. Therefore, if grouping in sections is applied and the proper position is adopted for the feedback thermocouples, the regeneration duration of large NEG pumps can be accurately calculated either by eq. (7), or by integrating eq. (5) in the

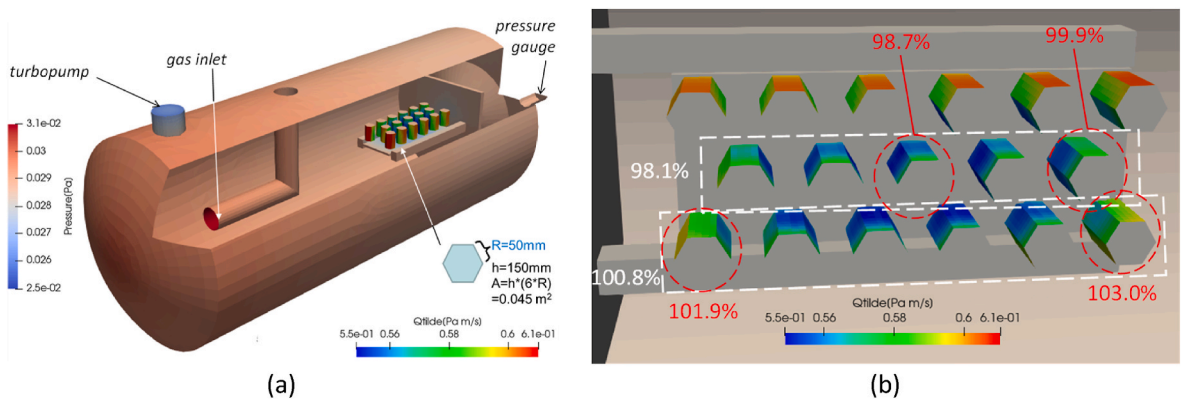

Fig. 14. (a) Cut view, contours of H_2 pressure in TIMO and passive structures (pressure contours in Pa), with contours of specific throughput at the open surfaces around each of the 17 cartridges. (b) view from the top, contours of specific gas throughput on NEG cartridges; at four cartridges, the throughput is presented in terms of percentage of the overall average throughput per cartridge, as well as for the central and lateral rows of cartridges. The gas injection is on the right hand side of the figure.

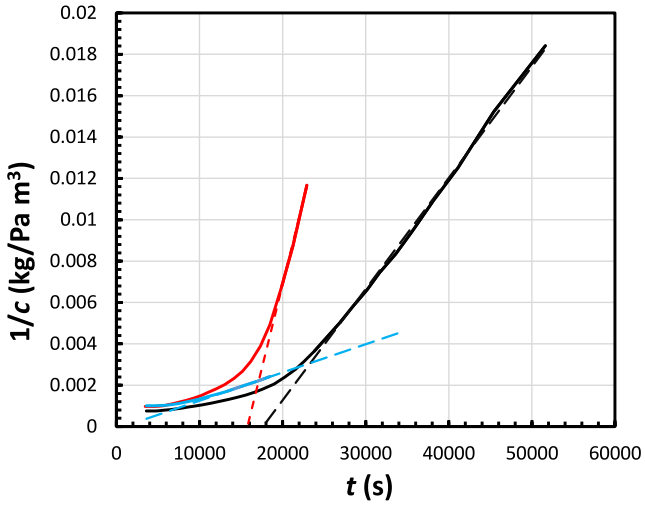

Fig. 15. Evolution of concentration during regenerations, derived from instantaneous pressure measurements, presented in form of inverse concentration versus time (solid lines); linear regression of the final phase of regenerations (dashed lines). Three nominal regeneration temperatures were considered: T = 600 °C (red), T = 550 °C (black), T = 500 °C (blue). Analyzing the slope of the curve provides the effective regeneration temperature.

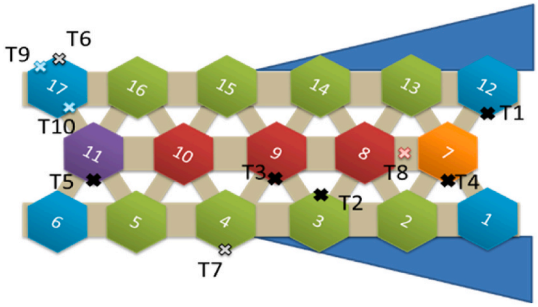

Fig. 16. Scheme of the mockup with five sections highlighted (marked by color), reporting also the position and number of thermocouples.

Table 6
Regression analysis to determine the effective temperature for the regeneration.

Nominal T	773 K (500 °C)	823 K (550 °C)	873 K (600 °C)
$10^{-7}\ a(T_{eff})$	1.37×10^{-7}	5.38×10^{-7}	16.23×10^{-7}
$k(T_{eff})$	1.33×10^{-6}	5.24×10^{-6}	1.58×10^{-5}
T_{eff}	766 K (99.1%)	817 K (99.3%)	865 K (98.9%)

case S_{aux} is expected to vary over time.

In general, the regeneration pressure was in the range 0.1–1 Pa, starting at a higher pressure and then decreasing with the decrease of concentration. A feedback scheme to maintain the regeneration pressure around a target value was also demonstrated with the mockup pump. As an example, during one regeneration test, the feedback control was capable of maintaining the regeneration pressure between 0.9 Pa and 1.05 Pa for a considerable part of the process. This result also demonstrated that the heating scheme and the thermal response of the system are adequate to maintain a given vessel pressure during regeneration, in order to operate the auxiliary pumps around their maximum throughput.

The results discussed here were confirmed by a dedicated test at 600 °C, in which the vessel was isolated during the heating phase, to avoid transient conditions at the beginning of the test. With an effective temperature of 858 K, and including the variable S_{aux} in the calculation, it was possible to reconstruct the real process, with the NEG concentration depleted from about 530 Pa m^3/kg to about 40 Pa m^3/kg, and a predicted total duration of 6.5 h while the real process took about 6.9 h. We should notice that an error might occur in the value of starting concentration for the above-mentioned reasons, i.e. uncertainties related to the values of TMP pumping speed.

4.4. Thermal aspects

The set of thermocouples and the grouping into sections of the mockup allowed to study the regeneration tests in TIMO with thermal models, in order to assess the main parameters required for reproducing the thermal equilibrium of the cartridges. The case of regeneration at nominal temperature of 550 °C is presented in Fig. 16; in this case, the mockup was equipped with all 34 cartridges, 17 cartridges per side. As expected, cartridges with higher neighboring index (such as the ones at the center) required a lower power to maintain the target temperature, while cartridges at the corner required the highest power, as summarized in Table 7. Cartridge n. 11 had a heater of different design. The control thermocouple T2 of the *green* group, was embedded in a stack oriented towards the inner side of the pump; it is possible to appreciate that T7, embedded on a stack oriented outwards, measured a 30 °C lower temperature (note that T2 had a significant level of noise with respect of the others). The same consideration holds for T1 with respect to T6, which were positioned in order to provide the highest and lowest stack temperature of the *blue* group, with a slightly higher temperature difference. Finally, again on the outer face of the corner cartridge, the grid temperature was T9 = 414 °C. The temperature inside the sandwich (T8) reached about 430 °C (almost at steady state after 4 h, and constant after 13 h of regeneration): as said, in that test cartridges were mounted on both sides of the support, and this justifies the relatively high temperature reached by that structure.

In the experimentally investigated configuration of 17 cartridges at steady state, similar results were obtained. A total heating power of 5450 W was necessary to sustain the nominal regeneration temperature of 550 °C. The corner cartridge had the external grid at a temperature T_{grid} = 415 °C. A thermal simulation with simplified bodies representing the cartridges was carried out, applying T_{grid} = 415 °C on the surface of the 17 radiative bodies and an effective emissivity of ε_{eff} = 0.95, thus obtaining a total heating power of 5900 W (see Fig. 17). Tuning the thermal model based on simplified geometries is important in order to prepare future studies of larger, multi-cartridge NEG pumps. Clearly, other combinations of ε_{eff} and cartridge temperatures can be found; to this regard, further studies shall be carried out to verify the best configuration capable of reproducing also the transient conditions. Optimizing the duration of the cooling down phase at the end of regenerations, which might be quite slow in the case of large pump assemblies, is key to maximize the availability of the pump.

Table 7
Average heating power and temperatures at steady state, for a regeneration at 550 °C nominal temperature.

Group	P[W]	control TCs	T[°C]	std dev [°C]
blue	322	T1	550	0.1
green	308	T2	548	9.4
orange	287	T3	550	3.9
red	256	T4	564	0.1
violet	317	T5	550	0.0
		extra TCs	**T[°C]**	
green		T7	523	
blue		T6	513	
sandwich		T8	432	
grid		T9	414	

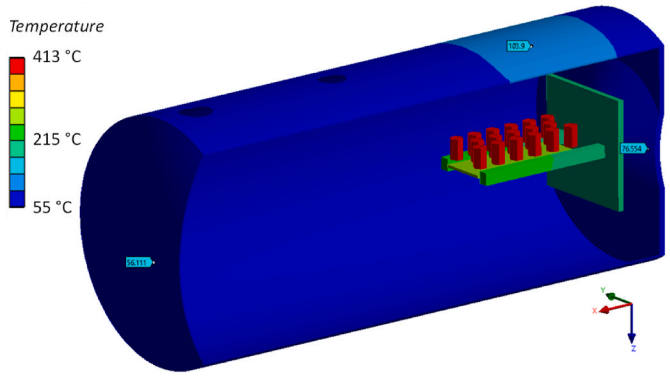

Fig. 17. Steady-state thermal simulation of the regeneration at 550 °C.

5. Perspectives and conclusions

The performances of sintered ZAO disks and of larger disk assemblies were studied. The design, construction and test of a large mockup pump was a fundamental step for the confirmation of the pumping performances in conditions relevant to fusion applications, such as in particular neutral beam injectors. It was shown that the pumping speed depends on many factors: operating pressure p, presence of i-th background gas, hydrogen concentration c, mass effect m. In the approximation of linearity, the installed pumping speed per cartridge can be estimated by superposing the effects. Using the symbols introduced previously, the pumping speed of each cartridge reads

$$S_{hex} = (A_N N \cdot \widetilde{S}(c) \cdot d_{cartr}) d_{multi} \cdot d_M d_p(p) \cdot \Pi_i d_i(t), \qquad \text{eq. 10}$$

with $A_N N$ the total surface of exposed NEG in one cartridge, and $\widetilde{S}$ the pumping speed per exposed disk area from eq. (9). The coefficient $d_{cartr} \approx 0.77$ accounts for the disk configuration inside one cartridge of this specific design (see section 2.2); the isotope coefficient is d_M (section 4.1); the effect of hydrogen pressure during adsorption is given by d_p, and the influence of the i-th getterable background gas over time is included in the term d_i (section 2.3). For a generic pump, the term which accounts for the multi-cartridge configuration and geometry d_{multi} is necessary to obtain the average effective pumping speed of one cartridges (section 4.2). Alternatively, $d_{multi} = 1$ if three-dimensional simulations are applied to simulate the effective pumping speed of a generic pattern of cartridges, as S_{hex} is applied directly on each cartridge. In the setup of the mockup pump, the spacing between cartridges is already a reasonable compromise between minimizing the "shadowing" effect, distributing uniformly the hydrogen load among cartridges, and providing a sufficient hydrogen capacity per unit volume.

The NEG regeneration was studied to verify equilibrium approximation (eq. (7)). Apart from the required speed - which normally defines the required number of sintered disks to be installed - the main factor determining the NEG pump design is the target duty cycle. In fact, as discussed previously, the duration of the hydrogen loading cycle defines the compromise on the getter mass for hydrogen capacity, and on the regeneration temperature to allow shorter or deeper regenerations. The possibility to predict the regeneration duration is fundamental for the design; it affects the electrical power and the power supplies, the auxiliary pumps, and the requirements for eventual thermal shields to protect in-vessel components with low temperature limit. Other constraints influencing the pump duty cycle may be given by safety regulations, in those cases for which limits on the total hydrogen contained in one vacuum vessel are requested, or limits to the tritium inventory. In addition, the possibility of water leaks shall be considered, for the risks they pose for NEG pumps (at the investment protection level). At the price of a slightly reduced speed, it might be advisable to operate the NEG at room temperature during the adsorption phase, because it corresponds to the NBI operation and therefore to a condition in which water leaks might occur. This is a concrete possibility, especially in the case of test benches dedicated to R&D related to high-power neutral beams.

As an example, we can discuss a hydrogen loading cycle of an NBI for DEMO. We will consider a scenario of relatively low gas load (e.g. with a laser neutralizer [30]): two NEG pumps could be adopted, one operating at 20–30 mPa and sorbing the gas injected in the beam source, and the second pump dedicated to maintain a higher vacuum for the neutral beam transport to the tokamak (of the order of millipascal). The possibility to separate the two volumes will be excluded. Assuming the same gas throughput as for the ITER beam source [46] of Q ≈ 3.6 Pa m^3/s of D_2, assuming RT operation, and taking the speed at $c = 650$ Pa m^3/kg as a minimum value before regeneration, according to eq. (10) about 300 cartridges are needed to provide the sufficient effective pumping speed. We shall also consider an initial concentration never below 130 Pa m^3/kg, to avoid the long duration of deeper regenerations. If only the pump dedicated to the beam source was regenerated, the target concentration would be reached after a cumulated beam duration of about 11 h; with a beam duty cycle of 0.3, this corresponds to about three days of pulsed operation. At a regeneration temperature of 600 °C, from eq. (7) the regeneration would last 11 h to decrease the concentration from 650 to 130 Pa m^3/kg under constant auxiliary pumping of 5 m^3/s. If a second NEG pump were present, dedicated to maintain low-pressure along the neutral beam transport region, it shall be designed for Q~0.8 Pa m^3/s of hydrogenic species from the tokamak, with a target vessel pressure of the order of ~2 mPa. A number of cartridges of about 500 is required; in that condition, the concentration of hydrogenic species does not vary much during the sorption phase, however during regeneration the gas in the two pumps – the one dedicated to the beam source and the one dedicated to the duct – will be redistributed and an average concentration will be obtained. In that case, the regeneration duration shall still be of the order of 10 h, to reach a uniform final concentration of 130 Pa m^3/kg but starting from a lower average concentration. More than 1 h shall be considered for heating the cartridges, and more than 6 h might be needed to cool down the getters below 100 °C, so that the pump would not be available for about one day for regeneration. At steady state, the heating power of about 300 W per cartridge is needed, totaling 260 kW; an energy of 3000 kW h would be used every 4 days, to be summed up to the power required for auxiliary pumping and for dedicated cooling systems, active during regeneration to protect other in-vessel components from possible overheating. Depending on the background gas composition, and on the time interval between regenerations, short reactivation cycles might be added, to restore the speed for hydrogen against the effect of other gases.

The results of the design, construction and tests of the mockup pump, that started in 2014 and was based on the improved properties of the sintered ZAO alloy [47], are now being considered for the development of large pumps in the field of nuclear fusion research. The advantages of a modular scheme based on multiple cartridges were shown. For the improvement of the vacuum system of the ITER prototype source SPIDER [48], the use of a large NEG pump (~300 m^3/s) was proposed and it is now in the phase of detail design [49]. A pump design was recently proposed for the Divertor Tokamak Test (DTT) [50]. In conclusion, the Non-Evaporable Getter technology was demonstrated as a promising technology for large pumps for hydrogenic species. At present, engineering research is focused on thermal aspects for the integration in large vacuum vessels, as well as safety aspects also related to possible water and air leaks, and on the optimization of the heating power supplies, to allow the deployment of very large NEG pumps.

CRediT authorship contribution statement

E. Sartori: Writing – review & editing, Writing – original draft-Writing – original draft, Visualization, Project administration, Methodology, Investigation, Formal analysis, Data curation, Conceptualization. **M. Siragusa:** Writing – review & editing, Validation, Methodology,

Investigation, Formal analysis, Data curation. **P. Sonato:** Writing – review & editing, Supervision, Funding acquisition, Conceptualization. **F. Siviero:** Writing – review & editing, Validation, Methodology, Investigation, Formal analysis, Data curation. **M. Mura:** Writing – review & editing, Project administration, Methodology, Investigation. **E. Maccallini:** Writing – review & editing, Methodology, Investigation. **A. Ferrara:** Writing – review & editing, Investigation. **P. Manini:** Writing – review & editing, Supervision, Methodology, Funding acquisition. **S. Hanke:** Writing – review & editing, Validation, Project administration, Methodology, Investigation, Formal analysis, Data curation. **C. Day:** Writing – review & editing, Supervision, Methodology, Funding acquisition.

Declaration of competing interest

The authors declare the following financial interests/personal relationships which may be considered as potential competing interests: Emanuele Sartori, Marco Siragusa, Piergiorgio Sonato, Stefan Hanke, Christian Day reports financial support was provided by European Consortium for the Development of Fusion Energy. Paolo Manini, Fabrizio Siviero, Piergiorgio Sonato has patent #WO2015198235 - GETTER PUMPING SYSTEM issued to SAES GETTERS S.P.A.

Data availability

Data will be made available on request.

Acknowledgements

This work has been carried out within the framework of the EUROfusion Consortium, funded by the European Union via the Euratom Research and Training Programme (Grant Agreement No 101052200 — EUROfusion). Views and opinions expressed are however those of the author(s) only and do not necessarily reflect those of the European Union or the European Commission. Neither the European Union nor the European Commission can be held responsible for them.

References

[1] E. Maccallini, et al., Non evaporable getter (NEG) technology: a powerful tool for UHV-XHV systems, AIP Conf. Proc. 1451 (2012) 24, https://doi.org/10.1063/1.4732360.
[2] P. Manini, A. Conte, L. Viale, A. Bonucci, L. Caruso, A novel route to compact, high performance pumping in UHV–XHV vacuum systems, Vacuum 94 (2013) 26–29, https://doi.org/10.1016/j.vacuum.2013.01.017.
[3] B. Ferrario, Chemical pumping in vacuum technology, Vacuum 47 (1996) 363–370, https://doi.org/10.1016/0042-207X(95)00252-9.
[4] C. Benvenuti, P. Chiggiato, P. Costa Pinto, A. Prodromides, V. Ruzinov, Influence of the substrate coating temperature on the vacuum properties of Ti–Zr–V non-evaporable getter films, Vacuum 71 (2003) 307–315, https://doi.org/10.1016/S0042-207X(02)00755-8.
[5] P. Chiggiato, P. Costa Pinto, Ti–Zr–V non-evaporable getter films: From development to large scale production for the Large Hadron Collider, Thin Solid Films 515 (2006) 382–388, https://doi.org/10.1016/j.tsf.2005.12.218.
[6] O.B. Malyshev, K.J. Middleman, J.S. Colligon, R. Valizadeh, Activation and measurement of nonevaporable getter films, J. Vac. Sci. Technol. A 27 (2009) 321–327. https://doi.org/10.1116/1.3081969.
[7] O.B. Malyshev, R. Valizadeh, J.S. Colligon, A. Hannah, K.J. Middleman, S. Patel, V. M. Vishnyakov, Influence of deposition pressure and pulsed dc sputtering on pumping properties of Ti–Zr–V nonevaporable getter films, J. Vac. Sci. Technol. A 27 (2009) 521, https://doi.org/10.1116/1.3112623.
[8] A.G. Mathewson, Synchrotron Radiat. News 3 (1990) 1.
[9] W.T. Shmayda, N.P. Kherani, A.G. Heics, Tritium removal from noble gas streams, J. Vacuum Sci. Technol. A 6 (1988) 1259–1262, https://doi.org/10.1116/1.575685.
[10] A. Santucci, et al., Novel non-evaporable getter materials and their possible use in fusion application for tritium recovery, Molecules 25 (23) (2020) 5675, https://doi.org/10.3390/molecules25235675.
[11] R.J. Kinze, J.L. Checchi, H.F. Dylla, Compatibility of the Zr-Al alloy with a tokamak plasma environment, J. Nucl. Mater. 103 (1981) 539–543, https://doi.org/10.1016/0022-3115(82)90655-9.
[12] M. Baquero-Ruiz, S. Coda, F. Dolizy, B. Duval, A. Fasoli, A. Ferrara, E. Maccallini, P. Manini, Y. Martin, M. Mura, H. Reimerdes, F. Siviero, Non-evaporable getter pump operations in the TCV tokamak, Fusion Eng. Des. 165 (2021), 112267, https://doi.org/10.1016/j.fusengdes.2021.112267.
[13] G. Motojima, et al., New installation of in-vessel Non Evaporable Getter (NEG) pumps for the divertor pump in the LHD, Fusion Eng. Des. 143 (2019) 226–231, https://doi.org/10.1016/j.fusengdes.2019.03.164.
[14] M. Audi, L. Dolcino, F. Doni, B. Ferrario, A new ultrahigh vacuum combination pump, J. Vac. Sci. Technol. A 5 (1987) 2587, https://doi.org/10.1116/1.574390.
[15] C.D. Park, S.M. Chung, P. Manini, Combination of compact nonevaporable getter and small ion pumps for ultrahigh vacuum systems, J. Vac. Sci. Technol. A 29 (2011), 011012, https://doi.org/10.1116/1.3529379.
[16] L.R. Grisham, et al., Recent improvements to the ITER neutral beam system design, Fusion Eng. Des. 87 (11) (2012) 1805–1815, https://doi.org/10.1016/j.fusengdes.2012.08.001.
[17] G. Serianni, et al., Neutralisation and transport of negative ion beams: physics and diagnostics, New J. Phys. 19 (4) (2017), 04500, https://doi.org/10.1088/1367-2630/aa64bd.
[18] R. Hemsworth, D. Boilson, P. Blatchford, M. Dalla Palma, G. Chitarin, H.P.L. de Esch, F. Geli, M. Dremel, J. Graceffa, D. Marcuzzi, Overview of the design of the ITER heating neutral beam injectors, New J. Phys. 19 (2017) 025005, doi: 10.1088/1367-2630/19/2/025005.
[19] M.J. Singh, D. Boilson, R.S. Hemsworth, et al., Powerloads on the front end components and the duct of the heating and diagnostic neutral beam lines at ITER, AIP Conf. Proc. 1655 (2015), 050011, https://doi.org/10.1063/1.4916468.
[20] A. Krylov, R.S. Hemsworth, Gas flow and related beam losses in the ITER neutral beam injector, Fusion Eng. Des. 81 (2006) 2239–2248, https://doi.org/10.1016/j.fusengdes.2006.03.006.
[21] P. Agostinetti, D. Aprile, V. Antoni, M. Cavenago, G. Chitarin, H.P.L. De Esch, Detailed design optimization of the MITICA negative ion accelerator in view of the ITER NBI, Nucl. Fusion 56 (1) (2015), 016015, https://doi.org/10.1088/0029-5515/56/1/016015.
[22] E. Sartori, et al., Simulation of space charge compensation in a multibeamlet negative ion beam, Rev. Sci. Instrum. 87 (2016), 02B917, https://doi.org/10.1063/1.4933252.
[23] M. Dremel, et al., Cryopump design for the ITER heating neutral beam injector, Nucl. Fusion 49 (2009), 075035, https://doi.org/10.1088/0029-5515/49/7/075035.
[24] M.Dremel, et al., Cryopump design development for the ITER neutral beam injectors, Fusion Eng. Des. 84 (2–6) (2009) 689–693, https://doi.org/10.1016/j.fusengdes.2009.01.004.
[25] G. Duesing, The vacuum systems of the nuclear fusion facility jet, Vacuum 37 (1987) 309–315, doi: 10.1016/0042-207X(87)90015-7.
[26] H. Zohm, et al., A stepladder approach to a tokamak fusion power plant, Nucl. Fusion 57 (2017), 086002, https://doi.org/10.1088/1741-4326/aa739e.
[27] D.R. Mikkelsen, C.E. Kessel, F.M. Poli, N. Bertelli, K. Kim, Survey of heating and current drive for K-DEMO, Nucl. Fusion 58 (2018) 036014.
[28] J. Chen, X. Jian, V.S. Chan, Z. Li, Z. Deng, G. Li, W. Guo, N. Shi, X. Chen, CFETR Physics Team, Self-consistent modeling of CFETR baseline scenarios for steady-state operation, Plasma Phys. Control. Fusion 59 (2017), 075005, https://doi.org/10.1088/1361-6587/aa6d20.
[29] P. Vincenzi, J.-F. Artaud, E. Fable, G. Giruzzi, M. Siccinio, H. Zohm, Neutral beam injection for DEMO alternative scenarios Fusion, Eng. Des. 163 (2021), 112119, https://doi.org/10.1016/j.fusengdes.2020.112119.
[30] P. Sonato, et al., Conceptual design of the DEMO neutral beam injectors: main developments and R&D achievements, Nucl. Fusion 57 (2017), 056026, https://doi.org/10.1088/1741-4326/aa6186.
[31] A. Simonin, et al., R&D around a photoneutralizer-based NBI system (Siphore) in view of a DEMO tokamak steady state fusion reactor, Nucl. Fusion 55 (2015), 123020, https://doi.org/10.1088/0029-5515/55/12/123020.
[32] C. Hopf, G. Starnella, N. den Harder, B. Heinemann, U. Fantz, A conceptual system design study for an NBI beamline for the European DEMO, Fusion Eng. Des. 146A (2019) 705-708 . https://doi.org/10.1016/j.fusengdes.2019.01.060.
[33] Patent WO2015075648, Non-evaporable getter alloys particularly suitable for hydrogen and carbon monoxide sorption. https://patentscope.wipo.int/search/en/detail.jsf?docId=WO2015075648. https://patentscope.wipo.int/search/en/detail.jsf?docId=WO2013175340. patent WO2013175340 "Non-evaporable getter alloys particularly suitable for hydrogen and nitrogen sorption".
[34] F. Siviero, et al., Characterization of ZAO® sintered getter material for use in fusion applications, Fusion Eng. Des. 146-B (2019) 1729–1732, https://doi.org/10.1016/j.fusengdes.2019.03.026.
[35] S. Hanke, et al., Experimental characterisation of a NEG pump of novel size – a major step to its application in DEMO neutral beam injectors, Energies 16 (7) (2023) 3148, https://doi.org/10.3390/en16073148.
[36] ASTM Standard F 798-97, Standard Practice for Determining Gettering Rate, Sorption Capacity, and Gas Content of Nonevaporable Getters in the Molecular Flow Region, American Society for Testing and Materials, West Conshohocken, PA, 1997. Withdrawn 2008).
[37] H. Yoshida, Testing of non-evaporable getter pills for standardization of their pumping performance testing method, Vacuum 197 (2022), 110797, https://doi.org/10.1016/j.vacuum.2021.110797.
[38] B. Erjavec, J. Setina, Investigations of a method for determining pumping speed and sorption capacity of nonevaporable getters based on in situ calibrated throughput, J. Vac. Sci. Technol. A 29 (2011), 051602, https://doi.org/10.1116/1.3626535.
[39] T. Feng, Y. Cheng, L. Chen, Z. Xi, J. Zhu, Y. Li, Hydrogen adsorption characteristics of Zr57V36Fe7 non-evaporable getters at low operating temperatures, Vacuum 154 (2018) 6–10, https://doi.org/10.1016/j.vacuum.2018.04.038.

[40] E. Sartori, P. Veltri, AVOCADO: A numerical code to calculate gas pressure distribution, Vacuum 90 (2013) 80–88, https://doi.org/10.1016/j.vacuum.2012.09.022.
[41] C. Day, X. Luo, A. Conte, A. Bonucci, P. Manini, Determination of the sticking probability of a Zr–V–Fe nonevaporable getter strip, J. Vac. Sci. Technol. A 25 (2007) 824, https://doi.org/10.1116/1.2748799.
[42] M. Siragusa, E. Sartori, M. Mura, F. Siviero, Numerical simulation of experimental tests performed on ZAO® non-evaporable-getter pump designed for neutral beam injector applications, Rev. Sci. Instrum. 91 (2) (2020), 023501, https://doi.org/10.1063/1.5128662.
[43] F.Siviero, et al., Robustness of ZAO based NEG pump solutions for fusion applications, Fusion Eng. Des. 166 (2021) 112306, https://doi.org/10.1016/j.fusengdes.2021.112306.
[44] M. Siragusa, P. Sonato, M. Visentin, M. Mura, F. Siviero, L. Viale, E. Maccallini, C. Day, S. Hanke, E. Sartori, Conceptual design of scalable vacuum pump to validate sintered getter technology for future NBI application, Fusion Eng. Des. 146 (2019) 87–90, https://doi.org/10.1016/j.fusengdes.2018.11.040.
[45] H. Haas, Chr Day, A. Mack, S. Methe, J.C. Boissin, P. Schummer, D.K. Murdoch, Test Facility TIMO for Testing the ITER Model Pump, 1999, pp. 1077–1080. IAEA-CSP-1/P; ITER-P2-08.
[46] E. Sartori, et al., Comparative study of beam losses and heat loads reduction methods in MITICA beam source, Rev. Sci. Instrum. 85 (2014), 02B308, https://doi.org/10.1063/1.4827677.
[47] Patent WO2015198235, Getter pumping system. https://patentscope.wipo.int/search/en/detail.jsf?docId=WO2015198235.
[48] E. Sartori, et al., First operations with caesium of the negative ion source SPIDER, Nucl. Fusion 62 (2022), 086022, https://doi.org/10.1088/1741-4326/ac715e.
[49] E Sartori, et al., Design of a large nonevaporable getter pump for the full size ITER beam source prototype, J. Vac. Sci. Technol. B 41 (2023), 034202, https://doi.org/10.1116/6.0002395.
[50] P Agostinetti, et al., Conceptual Design of the Gas Injection and Vacuum System for DTT NBI, Fusion Eng. Des. 192 (2023) 113638, https://doi.org/10.1016/j.fusengdes.2023.113638.